

# A method for in-vivo analysis for regional arterial wall material property alterations with atherosclerosis: preliminary results

K.B. Chandran<sup>ab,\*</sup>, J.H. Mun<sup>a,1</sup>, K.K. Choi<sup>b</sup>, J.S. Chen<sup>b</sup>, A. Hamilton<sup>c</sup>, A. Nagaraj<sup>c</sup>,  
D.D. McPherson<sup>c</sup>

<sup>a</sup> Department of Biomedical Engineering, University of Iowa, 1402 SC, Iowa City, Iowa, USA

<sup>b</sup> Department of Mechanical Engineering and Center for Computer-Aided Design, University of Iowa, 1402 SC, Iowa City, Iowa, USA

<sup>c</sup> Department of Internal Medicine and Feinberg Cardiovascular Research Institute, Northwestern University Medical School, Chicago, Illinois, USA

Received 9 April 2002; received in revised form 14 October 2002; accepted 30 October 2002

## Abstract

Atherosclerosis is a diffuse arterial disease developing over many years and resulting in a complicated three-dimensional arterial morphology. The arterial wall material properties have been demonstrated to show regional alterations with atheroma development and growth. We present a mechanical analysis of diseased arterial segments reconstructed from intravascular ultrasound images in order to quantitatively identify regional alterations in the elastic constants with atherosclerotic lesions. We employ a finite element and a displacement sensitivity analysis to divide the arterial segment into regions with different material properties and use an optimization algorithm to identify the elastic constants in these regions. The results with regional variations identified with this method correlated qualitatively with the extent and location of atherosclerotic lesions identified by visual inspection of the affected arteries. The optimized elastic modulus in regions affected by early atherosclerotic lesions ranged from 90.9 to 93.0 kPa where as the corresponding magnitudes in normal arterial segments ranged from 97.9 to 101.0 kPa. This method can be potentially employed to identify the extent and location of atherosclerotic lesions in a systematic analysis and may potentially be used for the early detection of lesion growth.

© 2003 IPPEM. Published by Elsevier Science Ltd. All rights reserved.

*Keywords:* Optimized elastic modulus; Early atherosclerotic lesions; Design sensitivity analysis

## 1. Introduction

The arterial wall is structurally inhomogeneous and exhibits incompressible and non-linear anisotropic material properties. The wall material constitutive relationship and the regional material property alterations with the onset of atherosclerotic lesions have been the subject of numerous investigations [1]. Arterial wall is a composite consisting of the intima, media, and the adventitia surrounded by the connective tissue. Classical

studies of Bergel [2,3] to determine the incremental elastic modulus with the assumption of an artery as a thick-walled isotropic and homogeneous non-linear elastic material have demonstrated that the arteries become stiffer with increased transmural pressure between 20 and 240 mm Hg. The constitutive relationship has been expressed with exponential [4], polynomial [5] and logarithmic [1] relationships for the above range of transmural pressures. The arterial wall has also been demonstrated to exhibit anisotropic behavior with varying elastic constants in the radial, circumferential, and axial directions [6,7] and requires identification of an increasing number of material constants in the constitutive relationship. On the other hand, Weizsacker and Pinto [8] as well as Dobrin [7] suggest that the arterial wall can be treated as isotropic within the physiological range of deformation.

Atherosclerosis is a diffuse and highly variable pro-

\* Corresponding author. Tel.: +1-319-335-5640; fax: +1-319-335-5631.

E-mail address: chandran@engineering.uiowa.edu (K.B. Chandran).

<sup>1</sup> Present address: Department of Bio-Mechatronic Engineering, College of Life Science and Technology, Sungkyunkwaa University, Suwon, Korea.

cess with lesion composition and distribution varying as a function of circumferential and axial location. This disease is characterized by the subintimal accumulation of extracellular lipids, fibrous tissue, smooth muscle cells, and calcium. Previous work has demonstrated that atherosclerosis alters normal arterial wall morphology [9] and mechanical properties [10,11]. Hayashi [1] reviewed studies evaluating the effect of atherosclerosis on vascular mechanics and the reported results were found to be conflicting and inconclusive. In atherosclerotic primate models, the elastic modulus has been shown to decrease with plaque development. Specifically, Hayashi et al. [12,13] and Pynadath and Mukherjee [14] have reported an increase in the elastic modulus with atherosclerosis, whereas other [15–17] report a decrease in stiffness with the disease. The conflicting reports can be attributed to the variations in experimental and analysis techniques employed, as well as variations in arteries and species studied.

In order to assess the arterial wall material properties and regional variations with the development of atherosclerotic lesions, the deformation pattern of the arterial segment must be measured for a specified load. Intravascular Ultrasound (IVUS) imaging provides comprehensive information connecting the 3D morphology and the deformation characteristics of the arterial segments [18]. Data obtained from IVUS images have been employed to determine the regional alterations in material properties with atherosclerotic lesions at various stages of development [19].

In our laboratory, we have reported on the 3D reconstruction of vascular segmental geometry from 2D ultrasound images coupled with mechanical analysis in order to assess regional changes in material property with atherosclerotic lesions. Vonesh et al. [20] obtained human arterial specimens postmortem from patients 50 years or older exhibiting varying degrees of atherosclerosis. The 3D reconstruction was obtained in an *in vitro* model where known transmural pressure loads were applied. Finite element analysis was performed to predict the 3D deformation of the segments with an assumed elastic constant throughout the segment and the same was compared with the measured deformation. An optimization algorithm was employed to alter the assumed elastic constants regionally to minimize the error between the computer predicted and actual deformation in order to assess segmental material property alterations. The regions with altered material property predicted by the analysis were correlated with histological data on the harvested specimens. The results predicted that the segments with early lipidous lesions become less stiff compared to non-diseased segments. However, Vonesh et al. [20] arbitrarily divided the arterial segment into four quadrants and analyzed material property differences between the preset regions.

Since atherosclerotic lesions are diffuse, such arbitrary

segmentation of the affected region is not a realistic representation of the complex geometry and material characteristics. An objective method must be developed to systematically specify different material properties for groups of finite element mesh to provide a more accurate representation of regional variations in the force-deformation behavior in normal and diseased segments. We present a technique incorporating a displacement sensitivity analysis in our methodology in order to achieve the stated goal and have demonstrated the feasibility of such an approach *in vivo* by employing an animal model of atherosclerosis.

## 2. Experiments and methods

### 2.1. *In vivo* data acquisition

For this study, Yucatan miniswine ( $n = 3$ ; weight 20–25 kg) were used. This animal model has been well established for developing atheroma similar to that found in human circulation. The institutional Animal Care and Use Committee of Northwestern University approved the animal studies. All animal and handling procedures strictly conformed to the “Guide for the care and use of laboratory animals” (National Institutes of Health Publication No. 85-23, 1996). After anesthetizing the animals, the right/left carotid and right/left femoral arteries were exposed with neck and groin incisions and markers placed under initial sterile surgery. These markers identified the region of endothelial denudation for subsequent IVUS imaging following the development of lesions. Due to endothelial denudation, these pigs develop atheroma at these locations. In this model, endothelial denudation with a high cholesterol diet causes atheroma formation similar, if not identical, to the atheroma formation in humans. Percutaneous angioplasty was performed in one carotid and one ileofemoral artery chosen randomly to denude the endothelium (contra-lateral arteries served as control). Following surgery, the animal was subjected to a hypercholesterolemic diet regimen for a period of six weeks for the development of atherosclerotic lesions similar to that in humans [21,22]. After the six-week period, the animal was prepared for acute surgery with appropriate anesthesia administration. A Millar pressure transducer (Millar Instruments, Inc., Houston, TX) was inserted through an arteriotomy and the blood pressure was recorded. An IVUS catheter (20 MHz, 3.2F; Boston Scientific Scimed, Maple Grove, MN) was then inserted through arteriotomy to image the vascular wall in the arterial segment of interest. The IVUS catheter probe was withdrawn at a constant rate of 0.5 mm/s while the images of the vascular segment were continuously recorded. ECG obtained during the experiments served as time reference between the recorded pressure signals and the IVUS images. An

example of an IVUS image with the intimal and adventitial border tracings along with the recorded ECG and pressure signals is included in Fig. 1. The heart rate in these animals ranged from 90–140 beats per minute (average—120 bpm). Given the pullback speed of 0.5 mm/s with 60 frames (30 images) per sec, we obtained data for two consecutive beats in 0.5 mm (1 sec) of the catheter pullback. Thus we obtain approximately 15 images in one cardiac cycle.

At the conclusion of the data acquisition, the animals were sacrificed with saturated KCl and the imaged arteries were excised. The intimal surface of the arteries was exposed by means of a longitudinal cut of the arterial segments and the intimal surfaces were visualized with the aid of a microscope for evidence of lesions.

Fatty and fibrofatty streaks and thrombi were easily differentiated on the intimal surface by this method. In cases where degrees of fibrofatty deposits were larger and could not be appropriately evaluated, the arterial segments were subsequently sectioned and evaluated under the microscope to determine if calcified components were also present within the fatty tissue. For early atheromatous lesions that were being qualitatively evaluated, this is an acceptable technique [23]. The extent and location of the lesions were schematically represented for subsequent comparison with the regions of optimized material properties used in the analysis described below. Visual inspection is a very good method to grossly determine the predominance of material type in the early atheroma (fibrous, fatty, or fibro-fatty). This qualitative description does not specify the exact percentage of each material component.

## 2.2. Optimization method for identification of vascular material property

The IVUS images were digitized from the resulting videotape at 1 mm intervals along the longitudinal axis over a 20 mm length of the employed arteries. The

arterial segments studied were relatively straight (no curvature). The catheter pullback will result in images obtained to be parallel to each other from the imaging catheter and were used for the reconstruction of the vascular segment geometry during the diastolic and systolic phases in the cardiac cycle. A three-dimensional Finite Element model with an assumed initial elastic constant was employed to compute the deformation of the vascular segment using the commercial finite element software ANSYS (version 5.5). The deformation of the reconstructed vascular geometry was computed from the end diastolic to the end systolic phase with the corresponding pulse pressure applied as the static load at the intimal surface. The computer predicted deformation of the geometry is compared with the measured deformation from the image data. A finite element mesh of the employed arterial structure consisted of 480 tetrahedron elements and 504 nodes, as shown in Fig. 2. A single layer of elements was used along the arterial wall thickness. The finite element input data was generated from each digitized slice such that each of 12 intimal and adventitial nodes were selected at 30 degree increments with respect to the origin at the center of the first slice using the Cartesian coordinate system. The arteries deform from the end diastolic to the end systolic geometry due to the pulse pressure applied as the load on the intimal surface. The pulse pressure measured from the recorded pressure signals was specified in the analysis. The wall material was assumed to be homogeneous, and isotropic with assumed initial Young's modulus (100 kPa). This value was chosen from the data for the Young's modulus under normal physiological pressure presented by Bergel [2]. The arterial wall was assumed to be nearly incompressible and hence a Poisson ratio of 0.49 was specified throughout the wall thickness. The optimization problem is based on the comparison of computed and measured displacement of the nodes from end diastole to end systole. In this analysis, we assume that the predominant deformation of the artery is in the radial direction and that any tangential

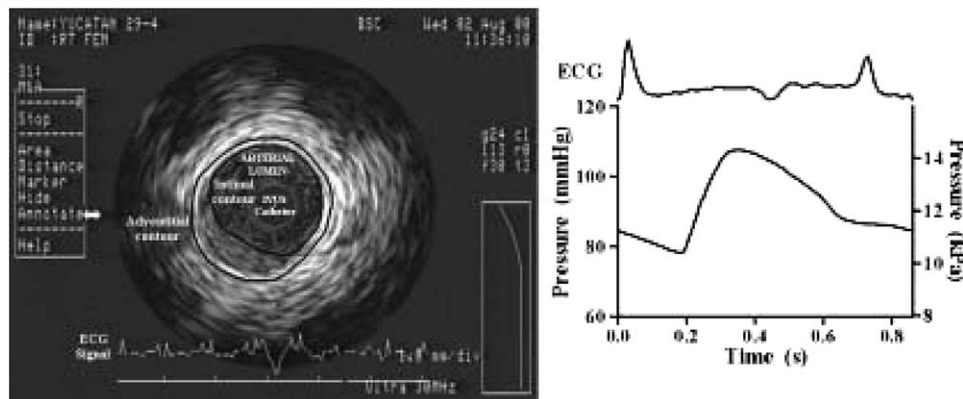


Fig. 1. An intravascular ultrasound image showing the cross-sectional view of a femoral artery and the manually traced intimal and adventitial contours (left), and the recorded ECG and pressure signals for the same artery (right).

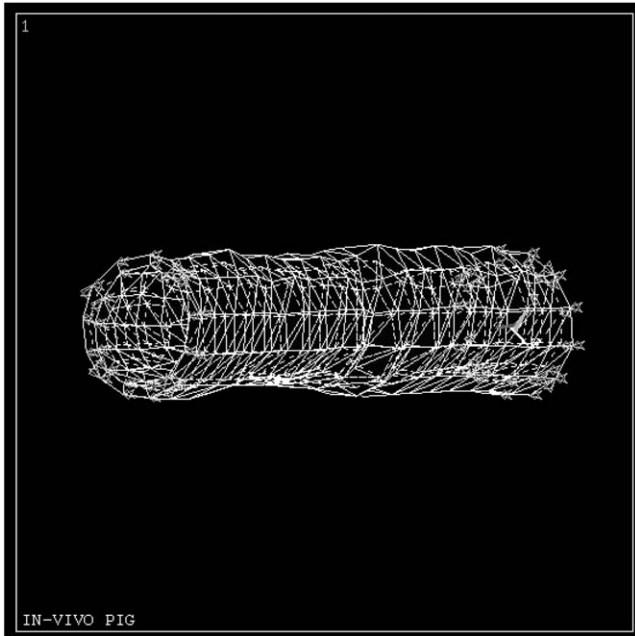


Fig. 2. Three-dimensional Finite Element model of an arterial segment generated from IVUS image data in vivo.

(rotational) motion is negligible. Nodes along the axial direction at the first and last slice were fixed as boundary conditions. That is, the proximal and distal ends of the arterial wall were fixed from movement along the axial direction. Additionally,  $x$ -direction movements of all nodes lying on the  $y$ -axis and  $y$ -direction movements of all nodes lying on the  $x$ -axis were constrained in the first and last slices in order to restrain rotation of the arteries during the deformation. The first two and last two slices (i.e., four out of 20) were not included in the optimization model to avoid errors due to the boundary condition restraints.

The difference in nodal displacements between the simulation model and the actual experimental data at the intimal and adventitial regions was calculated and defined as the error ‘e’ using the relationship

$$e = \tag{1}$$

$$\sum_{i=1}^m \sqrt{[u_i - (x_{is} - x_{id})]^2 + [v_i - (y_{is} - y_{id})]^2 + [w_i - (z_{is} - z_{id})]^2}$$

where,  $u_i$ ,  $v_i$  and  $w_i$  represent displacement of  $i^{th}$  node in the  $x$ ,  $y$  and  $z$  directions, respectively. In Eq. (1),  $x_{is}$ ,  $y_{is}$  and  $z_{is}$  are the experimentally measured end systolic stage coordinates of the  $i^{th}$  node, while  $x_{id}$ ,  $y_{id}$  and  $z_{id}$  are the end diastolic coordinates. The difference represents the actual displacement in the respective coordinate directions between end diastolic and end systolic stages.

A sensitivity analysis method was implemented to obtain sensitivities of displacements with respect to material properties. The resulting displacement sensi-

tivity values were employed to segment the arterial wall into various regions. Using the *Adjoint Variable* method, the sensitivity of the displacement  $u_i$  with respect to the Young’s modulus  $E_j$  at any finite element  $\Omega_j$  can be calculated using

$$\frac{\partial u_k}{\partial E_j} = - \int_{\Omega_j} \epsilon(\lambda) \frac{\partial \mathbf{C}}{\partial E_j} \epsilon(z) d\Omega \tag{2}$$

where  $\epsilon(\lambda)$  is the strain at element  $\Omega_j$  when a unit force is applied at node  $j$  along the direction of  $u_i$  and  $\mathbf{C}$  represents Modulus tensor for linear elasticity. In addition,  $\epsilon(z)$  is the computed strain at element  $\Omega_j$  for the originally applied load. Using the sensitivity Eq. (2), the following sensitivity matrix can be obtained:

$$\frac{\partial \mathbf{u}}{\partial \mathbf{E}} = \tag{3}$$

$$\begin{bmatrix} \frac{\partial u_1}{\partial E_1} & \frac{\partial v_1}{\partial E_1} & \frac{\partial w_1}{\partial E_1} & \frac{\partial u_2}{\partial E_1} & \dots & \frac{\partial u_m}{\partial E_1} & \frac{\partial v_m}{\partial E_1} & \frac{\partial w_m}{\partial E_1} \\ \vdots & \vdots & \vdots & \vdots & & \vdots & \vdots & \vdots \\ \frac{\partial u_1}{\partial E_i} & \frac{\partial v_1}{\partial E_i} & \frac{\partial w_1}{\partial E_i} & \dots & & \vdots & \vdots & \vdots \\ \vdots & \vdots & \vdots & & & \vdots & \vdots & \vdots \\ \frac{\partial u_1}{\partial E_n} & \frac{\partial v_1}{\partial E_n} & \frac{\partial w_1}{\partial E_n} & \dots & \dots & \frac{\partial u_m}{\partial E_n} & \frac{\partial v_m}{\partial E_n} & \frac{\partial w_m}{\partial E_n} \end{bmatrix}_{m \times 3m}$$

In Eq. (3),  $\mathbf{u} = [u_1, v_1, w_1, \dots, u_m, v_m, w_m]^T$ ,  $\mathbf{E} = [E_1, E_2, \dots, E_n]^T$ , where  $u_i$ ,  $v_i$  and  $w_i$  are the displacement of  $i^{th}$  node in the  $x$ ,  $y$ , and  $z$  directions, respectively, and  $m$  and  $n$  represent the total number of nodes and elements, respectively.

To make sure that accurate sensitivity is obtained, the sensitivity results in Eq. (3) that were obtained using the *Adjoint Variable* method in Eq. (2) were compared with the results of the Finite Difference method by perturbing the Young’s modulus of a typical atherosclerotic femoral arterial segment by 0.01, 1 and 5% and reasonable agreement was observed. In the comparison, 100% implies accurate sensitivity. For a randomly chosen node of a typical atherosclerotic femoral arterial segment, for instance, the comparison between the *Adjoint Variable* method and the Finite Difference method for the  $x$ -direction displacement sensitivity was 105, 124 and 128% with the perturbations of the Young’s modulus for the amounts of 0.01, 1 and 5%, respectively.

Before the optimization problem is formulated for the system identification, the arterial wall was divided into several regions based on the sensitivity information. For this purpose, the displacement in the radial direction of the employed artery at each node

$$r_i = \sqrt{u_i^2 + v_i^2} \tag{4}$$

is used. In Eq. (4), the displacement  $w_i$  in axial direction of the employed artery was not included since the value was significantly smaller compared to  $u_i$  and  $v_i$ . The design sensitivity of  $r_i$  in Eq. (4) is

$$\frac{\partial r_i}{\partial E_j} = \frac{1}{r_i} \left( u_i \frac{\partial u_i}{\partial E_j} + v_i \frac{\partial v_i}{\partial E_j} \right) \tag{5}$$

Then, each row of the sensitivity matrix in Eq. (3) was reduced into one value by adding the sensitivities in every row using the formula in Eq. (5) to obtain the column vector

$$\frac{\partial r}{\partial \mathbf{E}} = \begin{bmatrix} \sum_{i=1}^m \frac{\partial r_i}{\partial E_1} \\ \sum_{i=1}^m \frac{\partial r_i}{\partial E_2} \\ \vdots \\ \sum_{i=1}^m \frac{\partial r_i}{\partial E_l} \\ \vdots \\ \sum_{i=1}^m \frac{\partial r_i}{\partial E_n} \end{bmatrix}_{n \times 1} \quad (6)$$

where,

$$r = \sum_{i=1}^m r_i.$$

Using the sensitivity vector in Eq. (6), the regions are categorized based on the similar sensitivity values into 13 regions. The rationale behind this approach is that the system identification cost function in Eq. (1) is the sum of the square of the errors.

The system identification problem to determine the regional mechanical property of the employed artery based on the displacement sensitivity analysis can be defined by minimizing the cost function subject to the thirteen design variable constraints as

minimize  $e =$

$$\sum_{i=1}^m \sqrt{[u_i - (x_{is} - x_{id})]^2 + [v_i - (y_{is} - y_{id})]^2 + [w_i - (z_{is} - z_{id})]^2} \quad (7)$$

subject to

$$10^4 \leq E^i \leq 10^9 \text{ dyne/cm}^2,$$

$$i = 1, \dots, 13$$

For each 3-D arterial model, the Young's modulus  $E^i$ ,  $i = 1 - 13$ , was calculated for 13 discrete regions that was categorized based on the regional sensitivity factor ( $S_i$ ) for each group computed from Eq. (6). The system identification process using updated regional Young's modulus and regional sensitivity values are continued until the optimum cost is obtained. The detailed flow chart of the partitioning of the regions of arterial segment based on sensitivity analysis and system identification for regional material property assessment is provided in Fig. 3.

### 3. Results

In order to demonstrate the feasibility of the method for identifying normal and diseased segments, we applied this methodology to data obtained from three animals with induced atherosclerotic lesions. In one animal, the lesion was induced in one femoral artery while the contra-lateral artery was used as a control. In the other two animals, the lesion was introduced in one carotid while the contra-lateral artery was used as a control. Using the sensitivity and systems identification method described above, elastic moduli were determined for 13 regions in the normal and diseased arterial segments from these studies. Even though 13 regions were identified, our results showed that elastic constants in several regions were very close to each other. Hence, several adjacent regions with nearly equal elastic constants were coalesced such that in each arterial segment, three to five groups with different material properties were identified.

In order to display the regions with different material constants, a longitudinal cut was made on each artery model and the intimal surface of the left and right segments were displayed. Regions of different elastic constants were then displayed by color-coding as shown in Fig. 4. The corresponding elastic constants in these regions (mean  $\pm$  S.D.) are shown below each of the arterial segment figures. The results for the normal and diseased femoral arterial segments are displayed in Fig. 4A. The top left panel shows the material property distribution in the normal artery (right femoral) and the right panel for the artery (left femoral) with the lesion. The schematic representation of the extent and location of the fibrous/calcific plaque from the visual inspection in the left femoral artery is also included in the figure. In the right femoral artery, only thrombus or blood clot was observed without any atherosclerotic plaque in the arterial wall. In the normal artery, the material constants were similar in all the three regions with magnitudes close to 100 kPa whereas in the diseased segments, the elastic modulus in the regions shaded yellow were about 10% smaller than in the other regions. The magnitudes of the elastic modulus represented by the various colors are included below each of the figures for ease in interpretation. A qualitative correlation between the regions identified with reduced elastic constants and the region identified with fatty and fibrous plaques from visual inspection can be observed from this figure.

Similar results from the analysis of the two carotid vessels are displayed in Panels B and C in Fig. 4. In the case of the third animal, the image data from the normal artery was not used in the analysis. The image data for this case showed that the catheter and the artery were similar in size and the lumen was not visible. This is probably in part due to vasoconstriction around the catheter that we occasionally encounter. Once again, it can

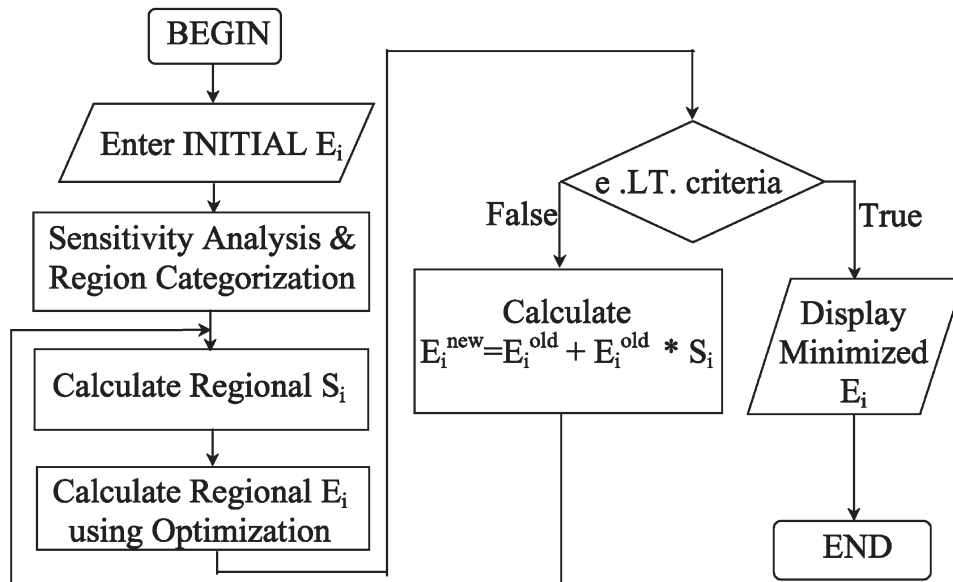


Fig. 3. Flow chart of numerical analysis algorithm including the partitioning the regions of arterial segment based on sensitivity analysis and system identification analysis of regional elastic modulus to minimize displacement error ( $S_i$  is the regional sensitivity factor).

be observed that in the normal carotid artery (animal 2), as verified by the visual inspection of the excised vessels to confirm the absence of atherosclerotic lesions, our analysis method results in a uniform material property throughout the segment. On the other hand, the material property demonstrated regional variations in segments with the presence of lesions, and a qualitative correlation between regions with reduced elastic constant values and the regions identified to have fibrous or lipidous plaques can be observed.

To demonstrate that the developed design sensitivity analysis and system identification technique to identify regional changes in arterial wall material properties with early atherosclerosis gives reasonable results, the absolute displacement error for each slice for a typical example of Femoral artery before and after the application of the analysis is given in Fig. 5. The error was normalized with respect to the mean diameter of the artery at end systole (4.3 mm for this artery). The normalized mean ( $\pm$  S.D.) error value was 1.1 ( $\pm$  0.43) with the initially assigned uniform mechanical property (100 kPa). After the optimized regional mechanical properties, the normalized mean ( $\pm$  S.D.) error value was reduced to 0.3 ( $\pm$  0.22).

#### 4. Discussion

We have presented a method for the systematic assessment of regional differences in the arterial wall material property with the development of atherosclerotic lesions. We have demonstrated the feasibility of the method in an animal model with early stages of atherosclerotic lesion development. Morphologically realistic three-dimen-

sional geometry of the carotid and femoral arterial segments in a miniswine model with induced atherosclerotic lesions was reconstructed from IVUS images. With the measured pulse pressure applied as the load in a finite element analysis and optimization algorithm, we computed the regional distribution of the elastic constants based on the minimization of the error between the computer predicted and the actual deformation of the vessel segment. In order to objectively divide the regions with different material properties, we employed a displacement sensitivity analysis. We demonstrated the feasibility of the method by applying this technique with data obtained from the femoral and carotid arteries with induced atherosclerosis in one artery while the contralateral artery served as control. In this preliminary study, we compared the results of different material property in various regions from the analysis of the diseased artery with the extent and location of the lesions identified by visual inspection. The results presented in this work demonstrated that:

1. The elastic constants in the normal artery did not exhibit regional variations. In the normal arteries without any atheroma lesions, regional differences in material property would not be anticipated.
2. In the case of arteries with early atherosclerotic lesions, our analysis identified regions with reduced elastic constants, and these regions qualitatively correlated with those visually identified with lipidous and fibrous early atherosclerotic lesions.

The intravascular ultrasound (IVUS) images presented in this study, we believe, can provide sufficient resolution for the miniswine animal model as outlined below.

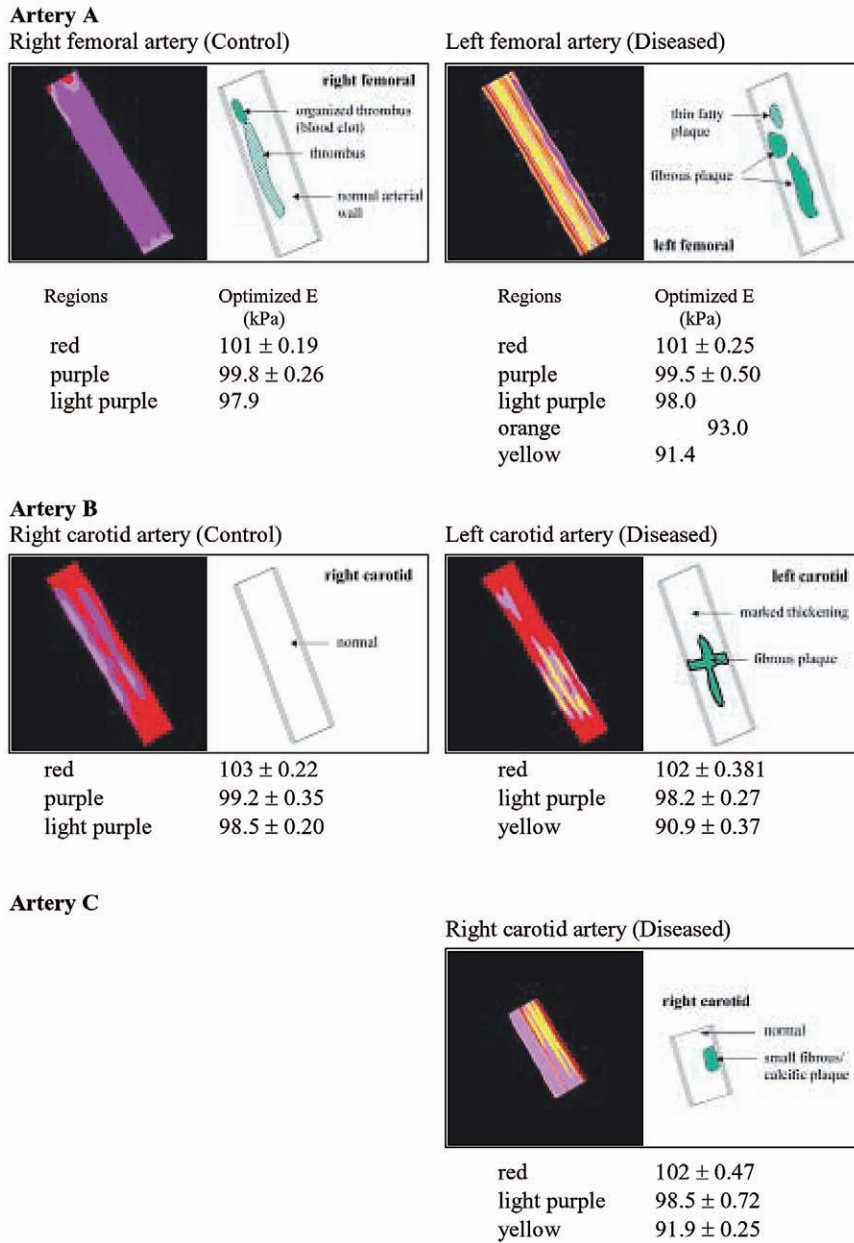


Fig. 4. Color-coded regional variation in arterial wall material property determined from the mechanical analysis compared with the corresponding schematic of the extent and location of the lesion determined from the visual inspection of the excised arterial specimens. Panel A: Femoral artery; Panel B and C: Carotid arteries. The left columns of Panels A and B demonstrate the material property distribution in normal (control) artery and the right column in arteries with the lesions. The magnitudes of the elastic constants are included below the figures.

The weight range for the animals was 20–25 kg and arterial diameter from 1.5 to 3.0 mm. The video monitor is approximately 512 × 512 pixels with the IVUS images approximately 400 × 400 pixels. The scan size was approximately 6 mm with a resolution set so that each mm is 70 pixels. Coronary arteries are known to increase 15% in a cardiac cycle and peripheral arteries by 20% in the absence of severe/diffuse atherosclerosis. Assuming a 20% change for these arteries throughout the cardiac cycle, this change is 7 pixels. Missing one pixel will cause an error of up to 15%. The measurement

error of 15% is a random error since some of the measurements will be larger and some smaller. The results of the measurements error is against finding a difference in the elastic modulus (it would tend to minimize the true difference) as it is a random error. It is likely that a random error of 15% will attenuate a true difference (of about 10% in this study) in the elastic modulus. However, the fact that we observed a consistent change in every artery of a similar degree suggests that it may indeed be a real change. A larger number of studies with histological analysis will help to quantitatively

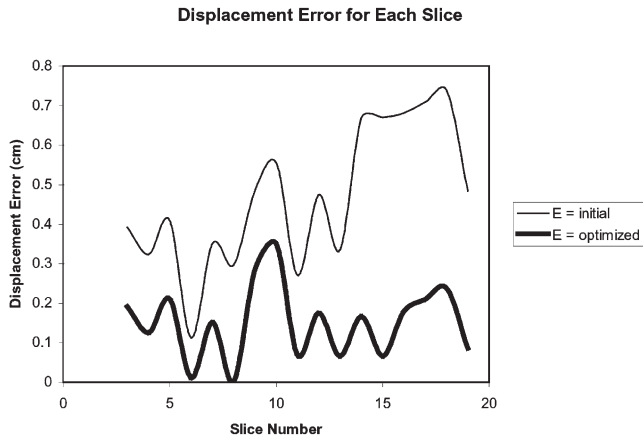


Fig. 5. Absolute displacement error for each slice for Femoral—1 (atherosclerotic) artery.

ively determine the statistical significance of the predicted elastic modulus alterations. With atheroma formation, the walls become thicker and the total arterial diameter increases (although the change in diameter over the cardiac cycle decreases). Hence we should be able to evaluate more mature atherosclerotic lesions in an easier and more accurate fashion. As the results are preliminary as indicated in the text, and normal wall thickness in this animal model is the “worst case scenario”, we believe that this methodology is acceptable and will be accurate to follow atheroma development.

A number of studies have been reported in the literature on the alterations in material properties with the onset and development of atherosclerotic disease. Most of the earlier work was confined to global changes in material properties at the site of the lesion. A review of the previous work by Hayashi [1] indicated that several of the published studies indicated stiffening of the artery with the lesion while others demonstrated a reduction in stiffness. The controversy on the direction of the material property alterations can be attributed to the segments and species studied, the stage of the growth of the lesion, as well as the analysis technique employed.

It is well known that the atherosclerotic lesions develop diffusely in arteries and result in a complicated three-dimensional morphology. Thus any material property alterations will also show regional variations and a more detailed analysis is necessary. Moreover, as the lesion develops from early involvement of lipids, developing into fibrous, fibro-fatty and calcific plaques, the material properties will also alter depending upon the stage of the development of the lesion. We have previously reported on a finite element analysis and optimization algorithm in order to determine the regional alteration in material properties with atheroma development [20]. By *in vitro* force-deformation studies on atherosclerotic cadaveric arteries, we demonstrated that the arterial wall becomes less stiff in regions with early atherosclerotic involvement, with a reduction in elastic

modulus of about 60% compared to those in the normal segments. However, in our mechanical analysis, we arbitrarily divided the vascular segment into four quadrants and restricted differences in elastic constants to those pre-specified regions. In the present work, we have removed that arbitrary division of the arterial segments into pre-specified number of regions by using a displacement sensitivity analysis technique.

It is important to compare the results from the present work with results reported previously. Lee et al. [11] determined the uniaxial compressive stiffness by *in vitro* mechanical testing of atheroma caps from the abdominal aorta of human specimens at autopsy and showed that fibrous and calcified caps were two and five times stiffer, respectively compared to non-fibrous caps. However, the same group [24] performing similar *in vitro* mechanical testing showed that the circumferential tangential modulus is not significantly affected by the degree of cellularity and calcification determined by histologic characterization. More recently, de Korte et al. [19] performed *in vitro* studies on diseased human femoral and coronary artery specimens subjected to static intraluminal pressures in the physiological range and measured the radial strains using IVUS elastography. With this method, they demonstrated that different strain values were found with fibrous, fibro-fatty, and fatty plaque components. Their results showing increased strain magnitudes (tissue becoming less stiff) with fibrous lesions qualitatively agree with the results of the present study. The computed pressure-strain modulus for the fibrous tissue was found to be about twice that for the fatty tissue. It should be noted that the pressure-strain modulus is computed from the change in radius for a given static transmural pressure, but does not take into account the thickness of the vessel wall. Hayashi et al. [13] induced atheroma in a rabbit model by using endothelial denudation and high cholesterol diet similar to that described in the present study. The vascular segments were excised from the animals and subjected to transmural pressures of 20, 100, and 180 mm Hg in an *in vitro* experimental set up. For each transmural pressure, the increase in diameter was measured and used in the calculation of the incremental elastic modulus. Their results suggested that the incremental elastic modulus increased by 50–100% in animals with vascular segments with greater than 80% area fraction stained by Sudan IV in histological analysis. The study described in the present work differs in two aspects from the studies described by de Korte et al. [19] and Hayashi et al. [13]. In the *in vitro* studies described by de Korte et al. and Hayashi et al., the connective tissue is removed from the excised arteries and the deformation measured *in vitro* under static transmural pressure loading. The deformation of the arteries measured *in vivo* in our study accounts for the effect of connective tissue and surrounding structures that the artery comes into contact. Our animal model for

inducing atherosclerosis was similar to that used by Hayashi et al. [13] even though we used a miniswine model compared to rabbit model used by Hayashi. In addition, we employed IVUS imaging in vivo to compute the deformation due to physiological pulsatile pressure and employed a finite element analysis to predict the regional variation in material properties. In this preliminary study, we did not perform a detailed histological study to differentiate between various components of atheroma quantitatively and hence we did not attempt to characterize the difference in material properties between fibrous, fatty, and fibro-fatty tissues. Our results suggest that the elastic modulus differed by about 10% in regions affected by atheroma compared to the normal arterial segments. As aptly pointed out by Hayashi et al. [13], the reported results are highly dependent upon the methods used for measurement and analysis of elastic properties, species, vascular site, and stage of atherosclerosis. Our methodology has the potential of analysis of regional differences in material properties with lesions at various stages of development utilizing in vivo ultrasound images and pressure data. This analysis technique may be potentially employed to detect the onset of lesions in early stages when interventions can be employed to arrest or reverse the process.

There are some limitations of the present study. In this preliminary analysis to establish the application of displacement sensitivity analysis with finite element and optimization algorithms to identify regional material property alterations, we did not perform detailed histological analysis to characterize or quantitatively determine the lesion extent and composition. A qualitative comparison of the results from the mechanical analysis to the regions identified with the presence of lesions from visual inspection demonstrates a reasonable correlation. Studies with detailed quantitative comparisons are necessary to further validate the method.

In this preliminary analysis, we also invoked several assumptions on the material characteristics of the arterial wall. Even though the wall is a non-linear anisotropic composite, we assumed the material to be linearly elastic in the deformation of the artery under physiological pulsatile pressure. Previous studies by Dobrin [7] as well as Weizsacker and Pinto [8] have suggested that under physiological loading, the arterial wall can be treated as isotropic. Our interest was to identify regions with *altered* material properties in the presence of a lesion. We therefore assumed the artery to behave as a linear elastic material where alterations in the Young's modulus can be analyzed using the method described in this study. The arterial wall is also known to be visco-elastic with the viscous component of about 10%. However, since we employed a static finite element analysis for the deformation between end diastole and end systole, the effect of viscosity was not incorporated in the present analysis. The arterial wall is also subjected to residual

stress [25,26] and it has been suggested that the residual stress will alter the pressure-deformation behavior of the arteries under physiological loading. Analysis performed in our laboratory has suggested that the effect of residual stress on the pressure-strain behavior under physiological loading [27] is only important in arteries where the wall thickness to radius ratio is less than about 0.07. Our aim was to assess alterations in material properties in regions with lesions relative to non-diseased wall regions. Accordingly we did not incorporate the effect of residual stress into this analysis.

In this preliminary study, we also assumed the arterial wall to be made of a single layer and hence alterations in material properties along the thickness of the vessel wall were neglected. More detailed histological studies to determine the lesion involvement along the wall thickness and repeating the analysis with several layers in the finite element model will be necessary to study the variation in the material properties along the wall thickness with lesions at various stages of development. As this was an initial attempt to determine in vivo material property determination, our data analysis was retrospective. We did not apply these methodologies prospectively on another data set to validate our results.

Incorporation of these features for a more quantitative characterization of the effect of lesion growth and development on regional alterations in wall material properties and prospective comparisons are ongoing in our laboratory.

## Acknowledgements

Partial support provided by a grant from the National Institutes of Health (NHLBI-HL62504) is gratefully acknowledged.

## References

- [1] Hayashi K. Experimental approaches on measuring the mechanical properties and constitutive laws of arterial walls. *J Biomech Eng* 1993;115:481–8.
- [2] Bergel DH. The static elastic properties of the arterial wall. *J Physiol* 1961;156:445–57.
- [3] Bergel DH. The dynamic elastic properties of the arterial wall. *J Physiol* 1961;156:458–69.
- [4] Fung YC. *Biomechanics: Mechanical properties of living tissues*. Berlin: Springer-Verlag, 1981.
- [5] Vaishnav RN, Vossoughi J, Patel DJ, Cothran LN, Coleman BR, Ison-Franklin EL. Effect of hypertension on elasticity and geometry of aortic tissue from dogs. *J Biomech Eng* 1990;112:70–4.
- [6] Patel DJ, Janicki JS, Vaishnav RN, Youg JT. Dynamic anisotropic viscoelastic properties of the aorta in living dogs. *Circulation Research* 1973;32:93–107.
- [7] Dobrin PB. Biaxial anisotropy of dog carotid artery: Estimation of circumferential elastic modulus. *J Biomech* 1986;19:351–8.

- [8] Weizsacker HW, Pinto JG. Isotropy and anisotropy of the arterial wall. *J Biomech* 1988;21:477–87.
- [9] Zarins CK, Giddens DP, Bharadvaj BK. Carotid bifurcation atherosclerosis-quantitative correlation of plaque localization with flow velocity profiles and wall shear stress. *Circulation* 1983;53:502.
- [10] Kitney RI, Moura L, Stranghan, K., 3-D visualization of arterial structures using ultrasound and voxel model. *Int J Cardiol Imaging* 1989;4:135–43.
- [11] Lee RT, Richardson SG, Loree HM, Grodzinsky AJ, Gharib SA, Schoen, F.J., et al., Prediction of mechanical properties of human atherosclerotic tissue by high-frequency intravascular ultrasound imaging: an in vitro study. *Intravascular Atherosclerosis and Thrombosis* 1992;12:1–5.
- [12] Hayashi K, Takamizawa K, Nakamura T, Kato T, Tsushima N. Effects of elastase on the stiffness and elastic properties of arterial walls in cholesterol-fed rabbits. *Atherosclerosis* 1987;66:259–67.
- [13] Hayashi K, Ide K, Matsumoto T. Aortic walls in atherosclerotic rabbits-mechanical study. *J Biomech Eng* 1994;116:284–93.
- [14] Pynadath T, Mukherjee DP. Dynamic mechanical properties of atherosclerotic aorta. *Atherosclerosis* 1977;26:311–8.
- [15] Haut RC, Garg BD, Metke M, Josa M, Kaye MP. Mechanical properties of the canine aorta following hypercholesterolemia. *J Biomech Eng* 1980;102:98–102.
- [16] Farrar DJ, Green HD, Wagner WD, Bond MG. Reduction in pulse wave velocity and improvement of aortic distensibility accompanying regression of atherosclerosis in the rhesus monkey. *Circulation Research* 1980;47:425–32.
- [17] Hudetz AG, Mark G, Kovach AG, Kerenyi T, Fody L, Monos E. Biomechanical properties of normal and fibrosclerotic human cerebral arteries. *Atherosclerosis* 1981;39:353–65.
- [18] Evans JL, Ng KH, Wiet SG, Vonesh MJ, Burns WB, Radvany MG et al. Accurate three-dimensional reconstruction of intravascular ultrasound data. Spatially correct three-dimensional reconstructions. *Circulation* 1996;93:567–76.
- [19] de Korte CL, Pasterkamp G, van der Steen AF, Woutman HA, Bom N. Characterization of plaque components with intravascular ultrasound elastography in human femoral and coronary arteries in vitro. *Circulation* 2000;102:617–23.
- [20] Vonesh MJ, Cho Jr. CH, Pinto JV, Kane BJ, Lee DS, Roth SI et al. Regional vascular mechanical properties by-3D intravascular ultrasound with finite-element analysis. *Am J Physiol (Heart Circ. Physiol. 41)* 1997;272:425–37.
- [21] Gal D, Rongione AJ, Slovenkai GA, DeJesus ST, Lucas A, Fields CD et al. Atherosclerotic Yucatan microsine: an animal model with high-grade, fibrocalcific, nonfatty lesions suitable for testing catheter-based interventions. *American Heart Journal* 1990;119:291–300.
- [22] White CJ, Ramee SR, Card HG, Abrahams LA, Svinarich JT, Wade CE. Laser angioplasty: An atherosclerotic swine model. *Laser in Surgery and Medicine* 1988;8:318–21.
- [23] Cotran RS, Kumar Kumar, Collins T, editors. Robbins pathological basis of disease. Philadelphia, PA: W.B. Saunders Co; 1999.
- [24] Loree HM, Grodzinsky AJ, Park SY, Gibson LJ, Lee RT. Static circumferential tangential elastic modulus of human atherosclerotic tissue. *J Biomech* 1994;27:195–204.
- [25] Fung YC. What are residual stresses doing in our blood vessels. *Ann Biomed Eng* 1991;19:237–49.
- [26] Vaishnav RN, Vassoughi J. Residual stress and strain in aortic segments. *J Biomech* 1987;20:235–9.
- [27] Mun JH, Chen JS, Chandran KB, Nagraj A, McPherson DD. Effect of residual stress on femoral arterial stress-strain behavior. *Korea Society for Mechanical Engineering International Journal* 2001;15:965–73.